



## Formation of twinned dendrites during unidirectional solidification of Al–32%Zn alloy

Zhong-wei CHEN, Jian-ping GAO

State Key Laboratory of Solidification Processing, Northwestern Polytechnical University, Xi'an 710072, China

Received 22 November 2016; accepted 7 July 2017

**Abstract:** The present study focused on the formation and crystallographic orientation of twinned dendrites coexisting with equiaxed grains in unidirectional solidification of Al–32%Zn (mass fraction) alloy. The morphology was investigated by optical metallograph and electron back-scattered diffraction technique. Results showed that the macrostructure of the alloy exhibited a typical feathery and fan-like structure while the microstructures were elongated lamellas, which were separated by coherent and incoherent twin boundaries. Both the primary trunk and all lateral arms of twinned dendrites grew along  $\langle 110 \rangle$  directions, unlike regular  $\langle 100 \rangle$   $\alpha(\text{Al})$  dendrites. The facet growth of crystals at solid/liquid interface was responsible for the origin of twinned dendrites during the weak local convection, and high thermal gradient and medium solidification velocity had significant contribution to the formation of twinned dendrites. The formation mechanism of twinned dendrites which consisted of three multiplication ways of new twin boundaries formation and one way of dendrite evolution in twin plane was shown schematically.

**Key words:** unidirectional solidification; twinned dendrite; growth direction; aluminum alloy

### 1 Introduction

The solidification microstructures in cast aluminium alloys are usually equiaxed dendrites and columnar crystals, which play an irreplaceable role in the materials performance that metallurgists want to make certain, both from the academic point of view and technological application [1]. Twinned dendrites, also called feathery grains, have been found in most semi-continuous castings and low speed tungsten inert gas welding aluminium alloys, and occasionally observed in Cu alloys [2–4]. Due to their deviant size and morphology, these grains result in deterioration of mechanical properties such as deformability and weldability of cast ingots, and thus it is crucial to understand the growth mechanism of this peculiar grain morphology [5].

Generally, dendrites often experience a competitive growth with columnar grains, but they depend on a number of factors during solidification processing [6]. The specific formation of twinned dendrites has been investigated under various process conditions, e.g., minimum solute concentration, relatively high rate of

solidification ( $R \approx 1$  mm/s), temperature gradient ( $G \approx 100$  K/cm), and necessary slight convection [7]. The critical concentration of elements needed for twinned dendrite formation in all kinds of binary alloys is almost different and varies with their distribution and diffusion coefficient in liquid metal. It is still unclear that which factor governs the growth direction or initiating twinning [8].

Theoretically, the twin phenomenon during metal solidification is considered as a result of stacking fault, which causes atomic rearrangement to form a new order with symmetry plane [9]. The formation of twinned dendrites in binary Al–Zn, Al–Mg, Al–Cu and Al–Ni alloys has been studied in specimens directionally solidified under identical thermal conditions with slight natural convection in the melt [10]. Nevertheless, the influence of the solute element nature and content has been found to be of less importance than that of the previously reported since feathery grains were formed in all four alloys. A detailed analysis confirmed that twinned dendrites grow along  $\langle 110 \rangle$  directions in all four cases. Therefore, twinned dendrites have been observed in most Al alloys whether stacking fault energy of the

alloys is high or low [10–12].

Researches on microstructures showed that twinned dendrites consist of a series of parallel thin lamellas, which have been separated by alternatively arranged smooth and rough boundaries [13]. In the meantime, as can be seen from longitudinal section, the twin grains develop from bottom position and expand to the whole ingot volume, always exhibiting a fan-shape characteristic when their macroscopic structure is observed. Considering the highly abnormal microstructures leading to undesirable segregation, recently, a divergence with respect to actual growth direction of twinned dendrite trunk along with either  $\langle 110 \rangle$  or  $\langle 112 \rangle$  direction has still remained a question, and the same case has been in the growth direction of secondary arms [6,14]. There are also different opinions regarding the origin and multiplication of twinned dendrites in Al alloys but main limit is the ingot consisting of many columnar grains [15]. Even though the coexistence of twinned dendrites with equiaxed grains in Al–4%Cu–0.24%Ti alloy ingot has been observed because of adding refiner Ti into melt, there is still lack of further systematic investigation [16].

A number of authors have also put forward three conjectures about tip shape of twinned dendrites, i.e., pointed, grooved and doublon tips, which can explain their growth advantage over regular  $\langle 100 \rangle$  columnar dendrite for a stable morphology [17]. Phase field simulations show that a grooved dendrite tip is not stable and quickly degenerates into a doublon-type dendrite in Al–30%Zn (mass fraction) alloy specimens [17]. Focused ion beam nanotomography and energy-dispersive spectroscopy chemical analysis in a transmission electron microscope reveal the existence of a positive solute gradient in a region localized within 2  $\mu\text{m}$  around the twin plane and support a doublon-type dendrite tip.

Aluminium alloys containing Zn as one of major alloying element in AA7000 series are widely used in aerospace, automotive and textile industries for their remarkable mechanical properties [18]. As far as binary Al–Zn alloys are concerned, twinned dendrites can be easily observed under 40% Zn (mass fraction) but above 10% Zn (mass fraction) partially, indicating that hexagonal close-packed structure Zn element has a tendency to modify the atomic arrangement locally and produce the twinning in Al alloys [10]. Additionally, according to GONZALES and RAPPAZ [19], the growth of regular  $\langle 100 \rangle$  dendrites at low Zn composition (typically  $C_{\text{Zn}} < 25\%$ ) is replaced by  $\langle 110 \rangle$  dendrites above 60% (mass fraction). Directionally solidified twinned samples of Al–23%Zn are partially remelted in a Bridgman furnace and then resolidified under controlled conditions, with minimal convection. It is found that,

although twin planes remain stable during partial remelting, non-twinned dendrites regrow during solidification [20]. Twinned dendrites appearing in an Al–26%Zn alloy have been quenched during growth and are then characterized as their side arms inclined at  $60^\circ$  from the trunk [21]. The results indicate that twinned dendrites probably have a growth advantage over those of regular dendrites which grow perpendicularly to the thermal gradient.

Keeping in view of the above, the binary Al–Zn alloy containing more Zn element (32%) was chosen to observe the twinned dendrites more clearly. This paper aimed to describe the structure and orientation features of twinned dendrites in macroscopic and microstructural views of different sections by optical metallograph and electron back-scatter diffraction technique. The emphasis of this work is to understand the mechanism of the origin of first twin plane and the development of fan-like structure.

## 2 Experimental

The Al–32%Zn alloy used in present study was prepared with pure elements (99.95% purity) in an electrical resistance furnace. The alloy ingots were produced to the dimensions of nearly 50 mm in diameter and 100 mm height by mechanical process for the laboratorial unidirectional solidification experiments. The schematic diagram of experimental setup used in this work is shown in Fig. 1, which can produce various temperature gradients and solidification velocities at different positions from chill plate [13], providing an integrated solidification condition for grain formation. The mold consisted of 2 mm-thick stainless steel wall, with 0.5 mm-thick heat resistance steel close to the bottom to achieve high heat extraction. The inner surface of lateral cylinder and bottom were coated with a thin layer of boron nitride to prevent pollution of impurity element and to unload the ingot easily.

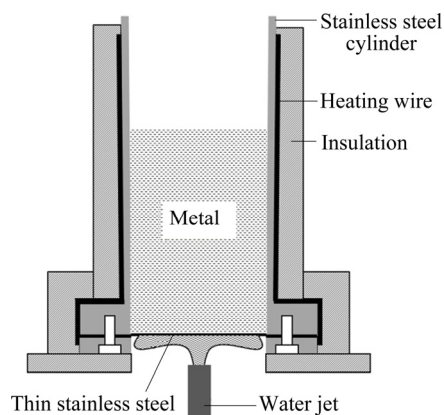


**Fig. 1** Schematic representation of unidirectional solidification apparatus

Firstly, the manufactured samples were introduced to furnace to melt by heating wire up to 100 K above the melting point of the alloy. Then, the melt was held about 5 min at 1000 K to eliminate force convection and homogenize. Lastly, heating electric power was shut down and water injection system at the mold bottom was switched on instantly in the melt solidification from chill plate. It should not be ignored that a slight convection is induced by thermal insulation of the lateral and top wall.

To observe the morphology of twinned dendrites, samples were cut along the longitudinal and transverse sections. The preparing procedure of the metallographic specimens was as follows: specimens were mechanically polished by fine SiC papers (from 80 to 2000 grade) using water as the lubricant, and then polished with diamond paste (0.5  $\mu\text{m}$  grade) using ethanol as the lubricant. Macrostructure was etched with Keller solution containing 2 mL HF, 3 mL HCl, 5 mL  $\text{HNO}_3$  and 100 mL  $\text{H}_2\text{O}$  for 5 min. In order to observe the twin planes, samples were etched with Keller reagent diluted with  $\text{H}_2\text{O}$  in a mass ratio of 1:10. For the purpose of revealing microstructure, the polished specimens were anodized at 30 V for 55 s in a solution containing 10 mL fluoroboric acid ( $\text{HBF}_4$ , 35% purity) and 390 mL  $\text{H}_2\text{O}$ . For electron back-scattered diffraction (EBSD) measurement preparation, no etching was needed on the specimens. In order to remove the small deformed layer of sample surface, electropolishing was performed on alloy at 10 V for 13 s in  $\text{A}_2$  solution, which consisted of

360 mL ethanol, 100 mL 2-butoxyethanol and 40 mL  $\text{HClO}_4$  [19].

Microstructures were characterized by Laser Tec C130 scanning confocal microscope and Leica DM4500 polarizing microscope. Crystal orientation measurements were performed on ZEISS SUPRA55 field emission gun scanning electron microscope installed with Channel 5 software for EBSD measurement.

### 3 Results and discussion

#### 3.1 Characterization of twinned dendrites

Three-dimensional macrostructure of the selected cubic bulk with a distance of 10 mm from the bottom of the Al–32%Zn alloy ingot is shown in Fig. 2(a). Once the twinned grains grow over equiaxed grains, the twin planes cross three sections as a number of straight lines. As their multiplication behavior proceeds densely, the twinned dendrites invade the whole ingot, finally exhibiting a typical feathery and fan-like structure, which makes a distinction with regular columnar dendrites. By observing the trace of twin plane in three sections, we found that growth directions of twinned dendrites are not aligned in vertical direction, as result of complexity of heat flux and nucleation site inclination in ingot. Figure 2(b) exhibits the microstructure of twinned dendrites etched with Keller reagent, which consists of alternately light and grey elongated lamellas in different orientations. The microstructure in Fig. 2(b) is a single

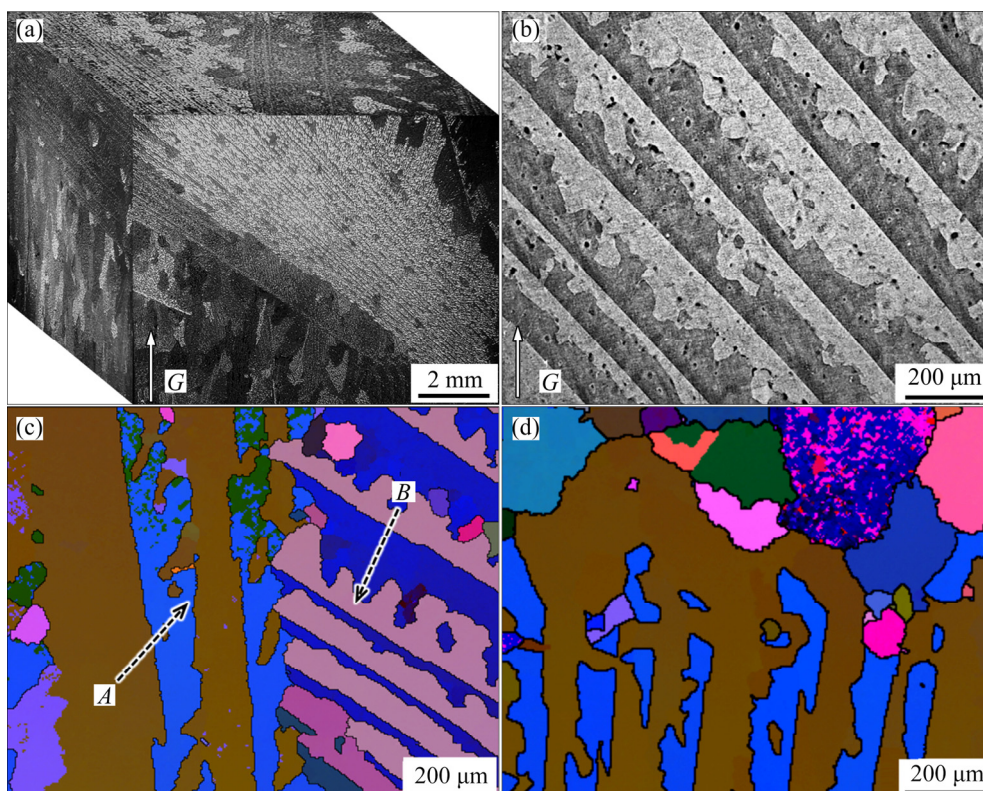


**Fig. 2** Structures of twinned dendrites in Al–32% Zn alloy: (a) Macrostructure; (b) Microstructure after Keller etching; (c, d) EBSD orientation distribution images

$\alpha(\text{Al})$  phase according to EDS and the cooling rate in this work. The straight line boundary in each pair lamella is the trace of twin plane propagation, while the wavy boundary corresponds to grain boundary as result of impingement of lateral arms.

Figure 2(c) shows two families of lamellae grains (*A* and *B*) revealed by EBSD. The two types of twinned grains are originated from different nuclei and region *B* is ultimately stopped by region *A* because main growth directions of the latter nearly align with the vertical thermal gradient. In other situation, twinned dendrites are stopped by equiaxed grains in tip region as observed in restructured EBSD orientation map (Fig. 2(d)). Growth advantages of half part between the twin boundaries are different, which can demonstrate the grooved tip morphologies [15]. The evolution of twinned dendrites always experiences a competitive growth during solidification process until the condition favors equiaxed grains over the twinned dendrites. Hence, the growth mechanism of twinned dendrites needs to be explained further.

### 3.2 Growth directions of twinned dendrites

To understand precisely the growth directions of twinned dendrites, the results on the twinned dendrites in three different sections with respect to direction of heat flux are shown in following text, including micrographs, EBSD orientation maps and the corresponding pole

figures.

Figure 3 shows the microstructure and the corresponding EBSD map of twinned dendrites in the section perpendicular to temperature gradient *G*. Figure 3(a) exhibits the metallographic structure of twinned dendrites, and the microstructure in the rectangle after anodic oxidation is zoomed in Fig. 3(b). This shows that secondary arms distribute symmetrically with respect to the twin plane, which is wholly different from regular columnar dendrites of typical crosses of  $\langle 100 \rangle$  growth direction. It is still a remarkable feature that the dendrite spacing  $\lambda_{\parallel}$  in one twin plane is far less than spacing  $\lambda_{\perp}$  between two twin planes, which might affect the solute content and its anisotropic rejection. As seen from the EBSD restructured map in Fig. 3(c), the twinned dendrites consist of two major colors corresponding to two orientations: the straight lines are the twin planes while the wavy boundaries represent the boundaries of twinned grains. Figure 3(d) shows characteristic distribution map of  $\Sigma 3$  grain boundaries. It is worth noticing that they belong to coherent and incoherent  $\{111\}$  twin boundaries, respectively. Sometimes twin plane is discontinuous and interrupted by an equiaxed grain as marked with an arrow in Fig. 3(c). This shows that the boundary of twinned dendrites contacting with equiaxed grains does not possess this twin relation, and there is a competitive growth of grains in the ingot. Therefore, morphology and structure of the twinned dendrites are

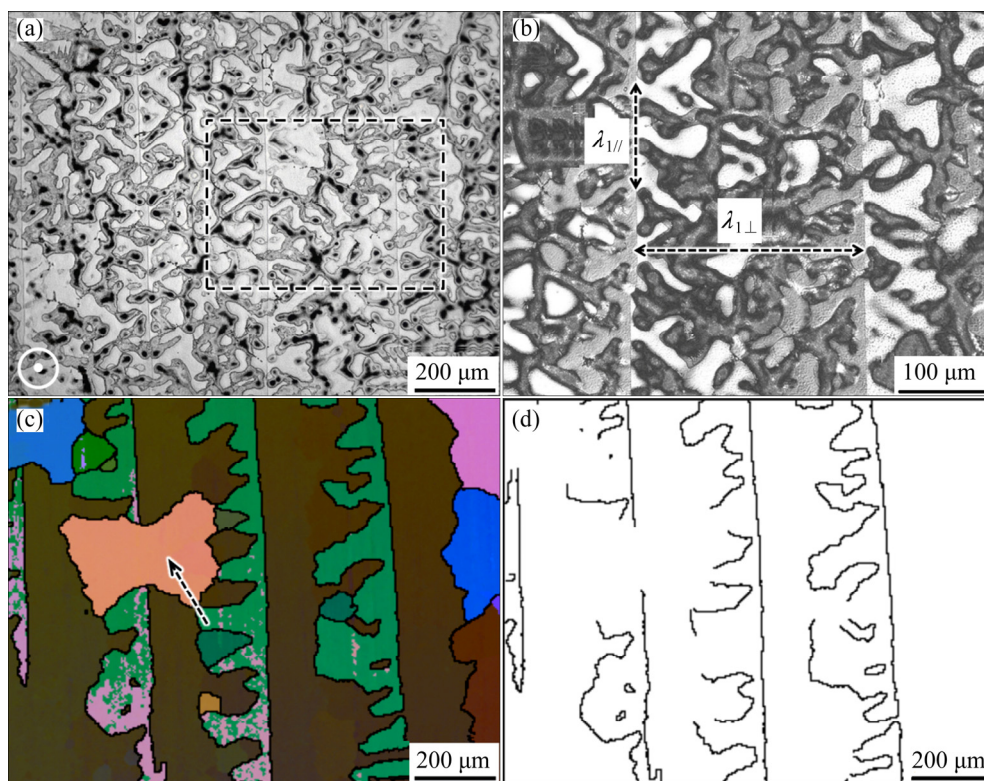


**Fig. 3** Twinned dendrites in section perpendicular to temperature gradient: (a) Microstructure; (b) Microstructure in rectangle of (a); (c) Corresponding EBSD orientation image of (a); (d)  $\Sigma 3$  grain boundary character distribution map of (b)

much more complex than ordinary  $\langle 100 \rangle$  dendrites and require further assessments.

In order to clarify the actual twin characteristic and avoid misunderstanding, Fig. 4 shows the microstructure, corresponding EBSD map and pole figures of the twinned dendrites on the longitudinal section nearly perpendicular to the twin plane and parallel to temperature gradient simultaneously. Figure 4(a) reveals the microstructure of twinned dendrite on this section. It can be seen that the twinned dendrites have relatively prosperous arms and their trunks are slender and more difficult to observe, while the lateral arms ( $OB$  or  $OC$ ) grow about  $60^\circ$  from the trunk ( $OA$ ). The corresponding EBSD orientation map in Fig. 4(b) presents a clear lamellar structure of the twinned dendrites, and there is slight orientation change less than  $10^\circ$  (existing sub-boundary between wathet and orange areas) in right part of the grain of twin plane. The elongated equiaxed grain can also be observed in the region, where the spacing of two successive coherent twin boundaries is pretty large, as shown by the right arrow. The discontinuity of twin plane also occurs, for example, the inflection point shown by the left arrow may be attributed to fluid motion during the early stages of solidification.  $\langle 110 \rangle$  pole figure drawn in Fig. 4(c) can

determine crystallographic relationships of lamellas to belong to one twinned dendrite, where each  $\langle 110 \rangle$  orientation is characterized by a small cloud of point. It is found that lamellas of one twinned dendrite share three  $\langle 110 \rangle$  poles and are marked with an arc, which is the trace of twin plane and can be easily speculated as  $\{111\}$ . Figure 4(d) gives the corresponding  $\langle 111 \rangle$  pole figure, and the  $\{111\}$  stereographic projection proves the above deduction.

In terms of dendrite growth direction, micrograph and its  $\langle 110 \rangle$  stereographic projection are analyzed together. For twinned dendrite labeled in Fig. 4(a), two secondary arms  $OB$ ,  $OC$  and trunk  $OA$  are exactly parallel to  $O'B'$ ,  $O'C'$  and  $O'A'$  in pole figure (Fig. 4(c)), respectively. Thus, side arms are confirmed growing along  $\langle 110 \rangle$  directions. With regard to trunk  $OA$ , it is not primary trunk of twinned dendrite but a side arm in twin planes since its projection is not the middle one of twin plane arc. At the same time, the left arm (dark blue orientation) and dendrite trunk make an angle with the observing section because their stereographic projections do not locate in big circle. As can be seen, the pole in the small circle of Fig. 4(d) is indeed a common  $[111]$  direction to both orange and blue lamellae of Fig. 4(b). The trace of the plane whose normal corresponds to this

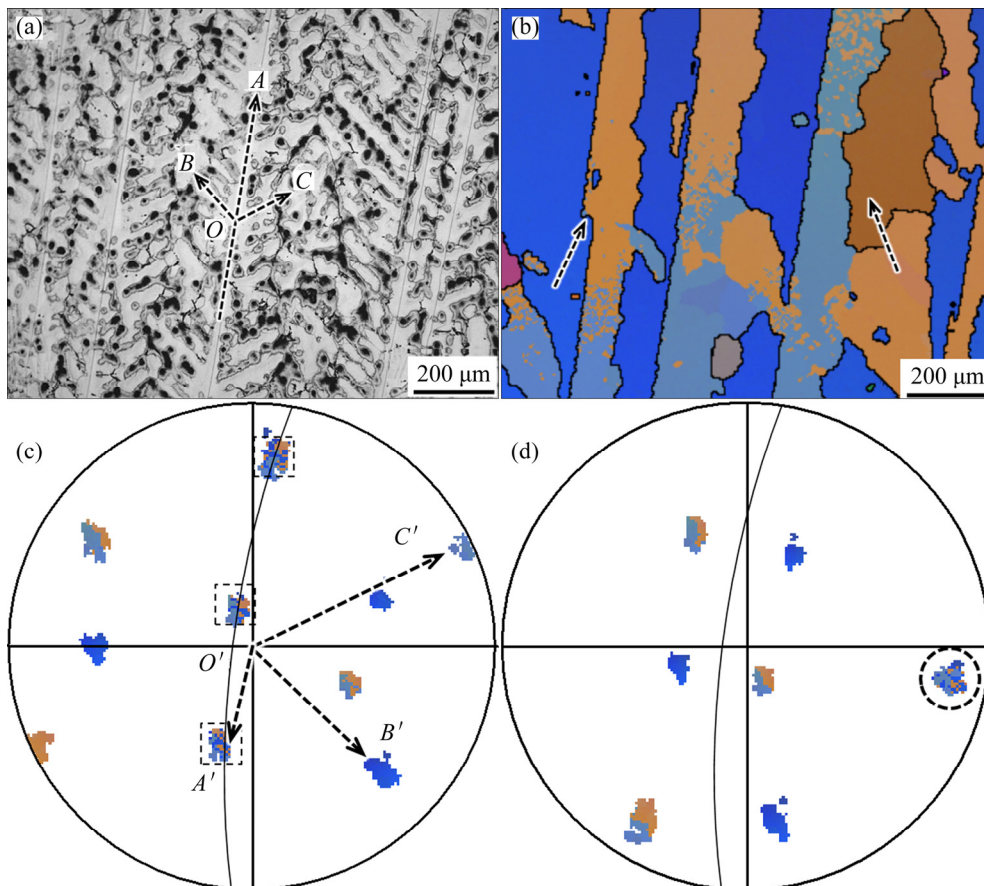


**Fig. 4** Twinned dendrites on longitudinal section nearly perpendicular to twin plane: (a) Microstructure; (b) Corresponding EBSD orientation image of (a); (c) Corresponding  $\langle 110 \rangle$  pole figure; (d) Corresponding  $\langle 111 \rangle$  pole figure

common [111] direction, is drawn as a circular arc in the pole figure. On the other hand, it can be verified easily that the three other pairs of  $\langle 111 \rangle$  directions corresponding to the orange and blue lamellae, are in a position of mirror symmetry with respect to the common (111) plane. Therefore, these lamellae are in a  $\Sigma 3$  twin relationship.

Microstructure and EBSD results of twinned dendrites in the longitudinal section nearly lying in twin plane are illustrated in Fig. 5 to determine the growth direction of twinned dendrite trunk. Micrograph in Fig. 5(a) shows a number of dendrites with coplanar trunk and side arms. It can be seen that dendrite arms completely develop and grow in  $60^\circ$  direction from

trunks, whose directions are slightly inclined to the left differing from the situation in Fig. 4(a). The orientation map of microstructure and corresponding  $\langle 110 \rangle$  pole figure are exhibited in Figs. 5(b) and (c), respectively. Because of machining error, the plane we observed was at several degrees (about  $8^\circ$ ) from the twin plane, and it can be seen that there were two kinds of orientation dendrites and three common pole points. The growth directions of primary trunk  $OD$  and two lateral arms  $OE$  and  $OF$  were identified by  $\langle 110 \rangle$  pole figure. It has been found that primary trunk and side arms coincide with  $O'D'$ ,  $O'E'$  and  $O'F'$  perfectly, in other words, parallel to them, respectively. It was believed that the primary trunks grow along  $\langle 110 \rangle$  direction and secondary arms also grow along  $\langle 110 \rangle$  regardless of lying in twin plane or not.

### 3.3 Origin of twinned dendrites

Figure 6 shows microstructures of ingot at different positions after anodic oxidation. Microstructure at the bottom of ingot is shown in Fig. 6(a), and a fine equiaxed zone resulted from suddenly high cooling rate by the direct contacting of melt and mould wall. The twinned dendrite nucleates at some distances from the chill plate, as shown in Fig. 6(b). Distribution of characteristic data of temperature gradient  $G$  and solidification rate  $R$  had been measured in this unidirectional solidification device [19].  $G$  value gradually decreased from high value by water cooling thin steel plate to about zero at the top due to thermal insulation. However,  $R$  value showed parabolic variation with the highest velocity at the bottom, higher one at the top, and lowest one in mid-height, which might have the intimate relationship with superheat degree of melt [19]. These factors produced favorable condition for twinned dendrites. In light of the thermal condition presented above, it could be suggested that the origin of twinned dendrite attributes to medium cooling rate. It had also been confirmed that twinned dendrites cannot be reproduced from remelted seed in Bridgman solidification experiment and regular dendrites grow epitaxially from twinned and untwinned parts [20]. Furthermore, the twinned dendrites do not only originate from normal equiaxed grains but also grow by accompanying with some unknown refining behaviors sufficient to completely suppress columnar growth. Hence, twinned grains originate from those equiaxed grains in heterogeneous nucleation way. Based on classical heterogeneous nucleation theory, the critical Gibbs free energy needed here becomes larger and then leads to the decrease of nucleation rate when considering the formation of twin boundary. Twin grain boundaries have lower energy as compared to other grain boundaries and could exist stably in the ingot. Therefore, the occurrence

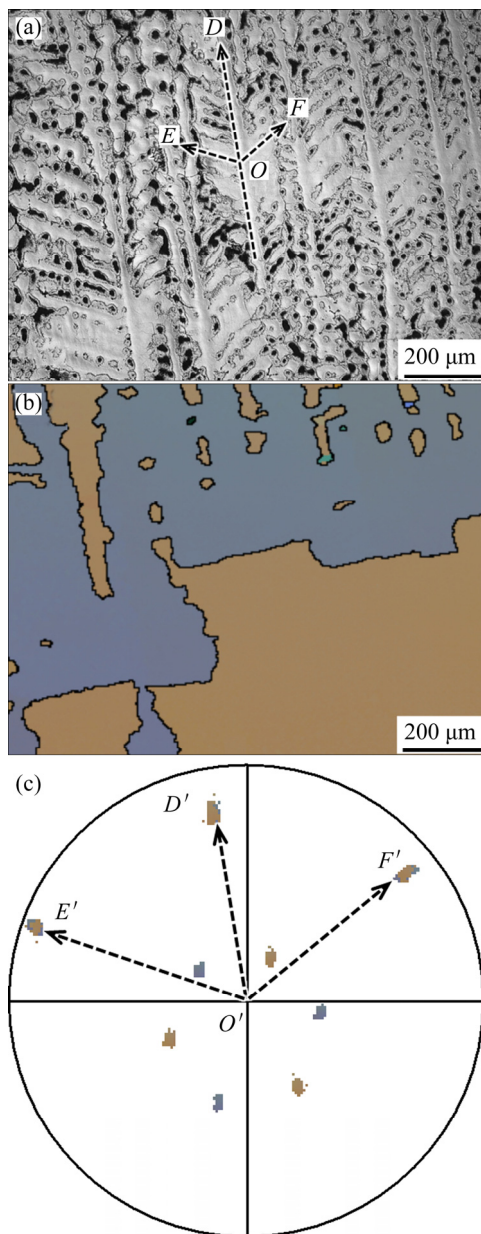


**Fig. 5** Twinned dendrites on longitudinal section nearly lying in twin plane: (a) Microstructure; (b) Corresponding EBSD orientation image; (c) Corresponding  $\langle 110 \rangle$  pole figure

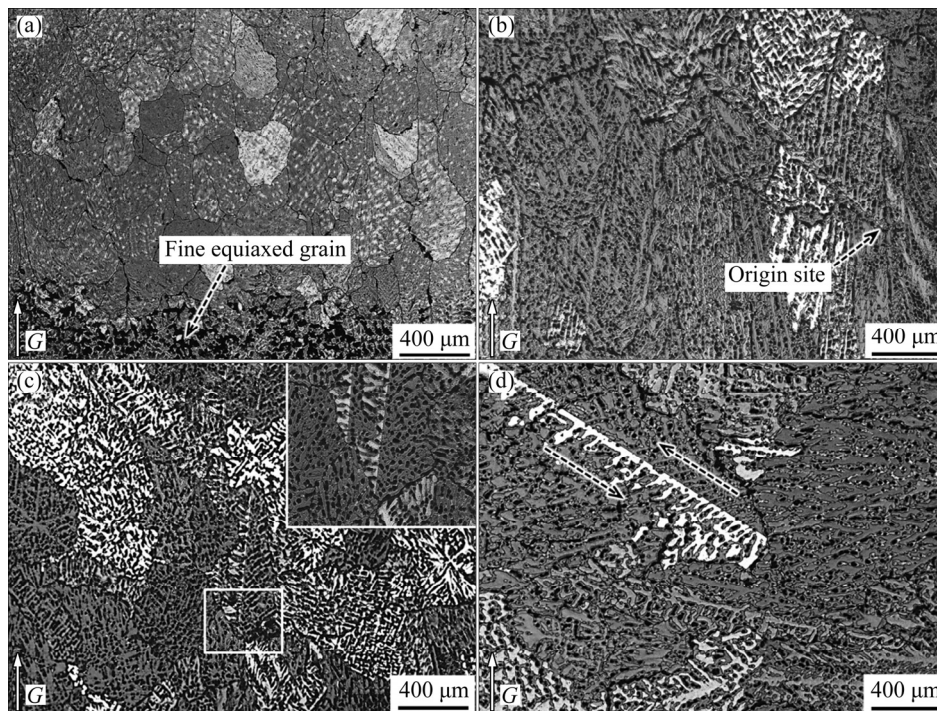


**Fig. 6** Microstructures at different positions of ingot after anodic oxidation: (a) At bottom; (b) Adjacent to bottom; (c) Origin site of twinned dendrites along near  $G$  direction; (d) Origin site of twinned dendrites in inclination direction

frequency of the twinned dendrites is far less than regular grains such as columnar crystals.

It was believed that twin boundary can form from the boundary, where two neighboring grains have particular orientation relation such as just rightly holding  $\{111\}$  plane in common direction, and are followed by incoherent grain boundary transforming into coherent twin boundary [22]. But as shown in Fig. 6(c), a straight twin boundary originates from one pre-existing grey grain and then another forms in a parallel direction, and top right corner shows the detail view of origin region. Twin boundary always presented a straight line from bottom to top, which had a contradiction with the former deduction [22]. Surrounding equiaxed grains and direction of twin plane almost grow stably along vertical thermal direction, which suggested that the intensity of present radial convection was weak. Normally, the non-faceted crystals in most metallic alloys with low fusion entropy have a rough interface at microscopic scale, where the effect of attachment kinetics was much lower, and growing twins should not exist but smooth dendrites always form under unidirectional solidification [23]. The present results showed that final morphology of crystal was affected not only by the fusion entropy but also by solute concentration and solidification undercooling.

Thus, one mechanism of this twinned grain formation was proposed here from Refs. [24,25]. Besides regular atomic arrangement at rough solid/liquid interface, there are still a number of disordered

arrangements of atoms near rough solid/liquid interface. The number of atomic layers in solid/liquid interface is proportional to the degree of interface undercooling. When thermal gradient is high, the corresponding sufficient low interface undercooling of rough interface with monoatomic layer can transform into local smooth interface when the desirable thickness reaches. Therefore, the alloys with low fusion entropy can grow according to the way of lateral extension growth of every step.  $\{111\}$  plane exposes at interface with a direction parallel to the direction of maximum interface energy, and then atom attaches on this facet plane with a twin relationship. Meanwhile, it can be inferred that necessary solute existence influences the atom adsorption and reduces the roughness at the atomic scale interface to promote the formation of twins.

One interesting circumstance of twinned grains found in Fig. 6(d) is that the dendrite arms between the twin planes had different growth directions. Observing the severe inclination of primary trunk and surrounding else equiaxed grains, we found that there was complex convection in this region. Because the local convection favored the dendrite arms that had growth direction opposite to the incoming flow (labeled with two arrows), the twinned grain formation can be attributed to the shearing force produced by melt flow [5]. It was worth noticing that the indexes of twin plane correspond to the slide plane  $\{111\}$  for face centered cubic (FCC) metal and the direction of primary trunk to the slide direction  $\langle 110 \rangle$  rather than the usual deformation twin

direction  $\langle 112 \rangle$ .

It was well accepted that twinning occurrence can be favored by the high temperature gradient condition as it can provide small curvature undercooling in favor of  $\langle 110 \rangle$  dendrites growth [23]. Besides, the position that has high growth rate may switch the regular dendrite direction from  $\langle 100 \rangle$  to  $\langle 110 \rangle$  aligning with the direction of heat flux. This transition might be dominated by the kinetic anisotropy leading to  $\langle 110 \rangle$  growth direction at intermediate velocity and  $\langle 111 \rangle$  growth direction at very high velocity rather than by surface energy anisotropy for favoring  $\langle 100 \rangle$  at low velocity [26]. More importantly,  $\langle 110 \rangle$  growth direction contributes to the formation of the  $\{111\}$  plane, while the growth in  $\langle 100 \rangle$  direction could not contain the twin planes.

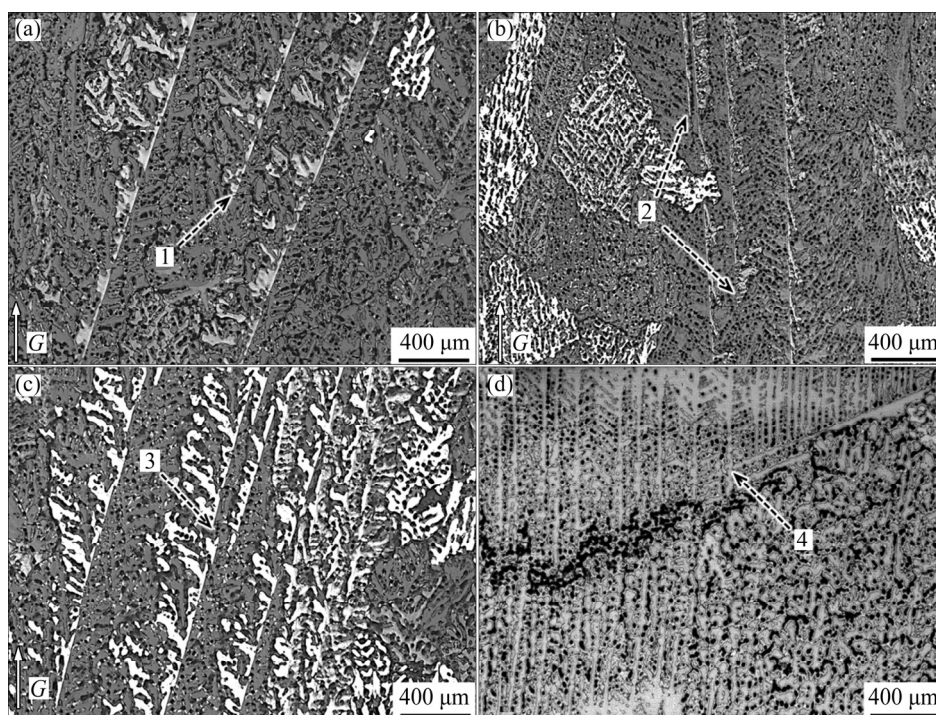
### 3.4 Multiplication of twinned dendrites

Figure 7 illustrates the multiplication behavior of twinned dendrites, and the schematic views of above four multiplication mechanisms are shown in Fig. 8. As single twinned dendrite began to grow, numerous lamellae of twinned grains successively formed in almost parallel direction. As shown in Figs. 7(a) and 8(a), a new twin boundary (labeled with arrow 1) originates from the region and separates two preexisting twin dendrites. Owing to the large spacing and collision of inner side lateral arms of two twinned dendrites, many fine equiaxed grains form in this region and then probably provide the twin condition since their orientation relation correlates with dendrite on one side of twin plane. The

mechanism of this case proved original alternate arrangement of light and grey regions separated by straight and wavy boundaries.

As seen in Figs. 7(b) and 8(b), two tertiary arms (labeled with arrow 2) parallel to the original twin plane grow and then become a new twinned dendrite trunk subsequently. Results showed that common type of new twin dendrite forms in secondary branch when the spacing of twin plane is relatively small and dendritic arms grow extensively. This multiplication attributes to the fact that the stacking fault occurs frequently and  $\{111\}$  twin planes formed spontaneously on lateral arms arise [14]. It should be noted that the energy needed here is much less than that of nucleating from equiaxed or columnar grains. Along with this multiplication behavior, the growth of primitive arms is usually hindered by new twinned dendrites.

Figures 7(c) and 8(c) reveal the propagation of lateral arms when the primary twinned dendrite trunk is discontinuous. Discontinuous coherent twin boundaries appear as a result of the grey part and light part of lamellae between twin planes corresponding to different undercooling. The grey part grows at lower temperature as it is located below the twin planes and grows preferentially. Obviously, the right half part (grey area) intrudes into left part (light area) and then facilitates the formation of new twin boundary (labeled with arrow 3) in contact zone. The encounter of the 15th arms on the right and tertiary arm on the left might occur in the direction parallel to original twin plane direction similar



**Fig. 7** Microstructures related to multiplication of twin dendrites: (a–c) On longitudinal section perpendicular to twin plane; (d) On section parallel to twin plane

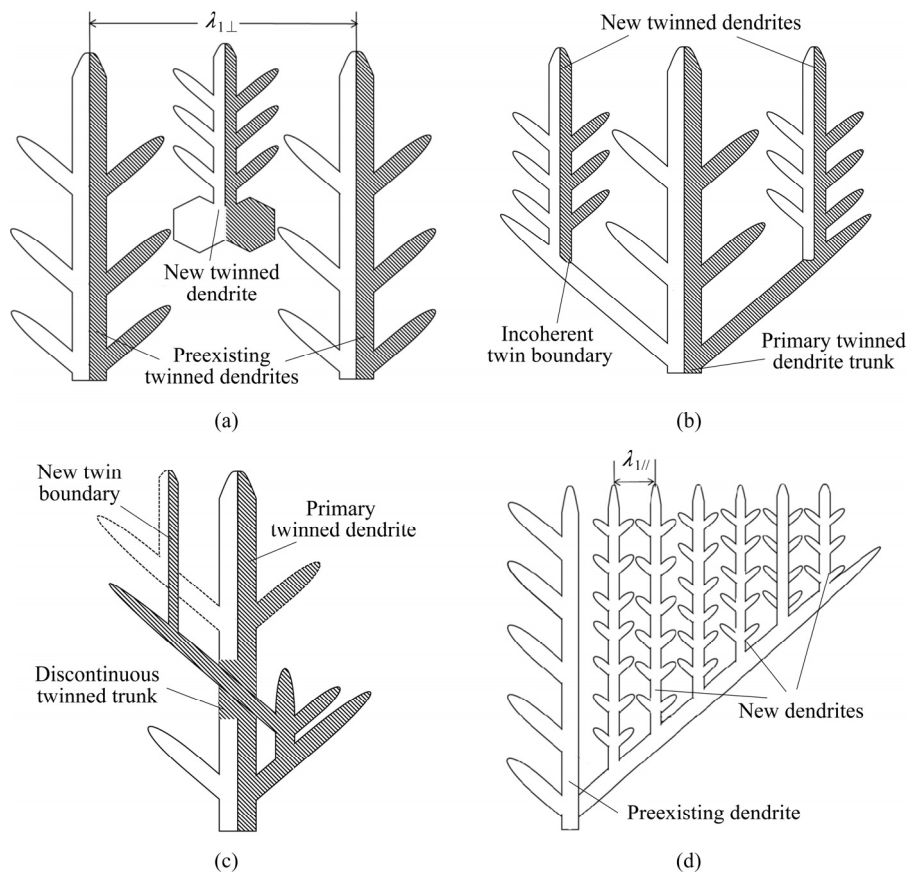


**Fig. 8** Schematic views of multiplication for twinned dendrites: (a–d) corresponding to cases of Figs. 7(a–d), respectively

to the analysis performed by SALGADO-ORDORICA et al [21]. In addition, it was worth noticing that the boundary where new twin dendrite formed is incoherent twin boundary, as shown in Figs. 8(a)–(c).

Figure 7(d) shows the dendrite multiplication way in the twin plane. The black area in Fig. 7(d) should be casting defects, such as the shrinkage and the inclusions. It can be seen that the growth on one side of lateral arms in twin plane is far extensive. After that, a plenty of new dendrites without fully arms (labeled with arrow 4) are readily formed on the long arm analogously to regular dendrite, as shown in Fig. 8(d). Firstly, it can be deduced that final constituent of dendrites in the twin plane is higher order branches of one side of initial twinned dendrite, and of course has smaller dendrite spacing compared to primary twinned dendrite trunk spacing. Secondly, the spacing of primary trunks perpendicular to twin plane is directly proportional to the distance from nucleating site since the twin planes deviate from vertical axis and the multiplication occurs in interval area. Lastly, the spacing of element segregation between twin planes is wider than that of dendrites in twin plane due to their complex branch morphology. Thus, the relationship between dendrite spacing  $\lambda_{1//}$  and plane spacing  $\lambda_{1\perp}$  between two initial successive rows depends on the height from nucleation site.

## 4 Conclusions

1) The macrostructure of Al–32%Zn alloy shows a feathery feature with fan shape owing to the abundant multiplications of twin boundaries, while microstructure appears as alternating light and grey bands with straight and wavy grain boundaries, which belong to coherent and incoherent  $\Sigma 3$  twin boundaries, respectively.

2) In terms of growth direction, the characterization of optical micrographs and the corresponding EBSD results show that primary twinned dendrite trunk cannot grow along the usual  $\langle 100 \rangle$  or  $\langle 112 \rangle$  crystallographic directions but along  $\langle 110 \rangle$  direction, and lateral arms also along  $\langle 110 \rangle$  directions no matter they are in twin plane or not.

3) Two mechanisms are proposed with respect to the origin of the twinned dendrites. The twinned dendrites may be produced from facet growth of crystals when the local convection is weak, and the twinned dendrites originate from shear force induced by relatively strong convection. High thermal gradient and medium solidification velocity have significant contribution to the formation of twinned dendrites.

4) New twin dendrites regenerate in a region where the spacing of twin plane is large, propagate from secondary arm directly, and occasionally grow by

merging of two higher order arms. Dendrite multiplication process in the twin plane is similar to the regular dendrites but occurs easily than twinned dendrites. The above results can also explain the difference in  $\lambda_{1//}$  and  $\lambda_{1\perp}$  directly.

## References

- [1] RAPPAZ M, GANDIN C A, DESBIOLLES J L, THÉVOZ P. Prediction of grain structures in various solidification processes [J]. Metallurgical and Materials Transactions A, 1996, 27(3): 695–705.
- [2] LAST H R, SANDERS T H, GONSALVES J M. Stability of microstructures in chill-cast aluminum alloys containing twinned columnar growth structures [J]. Metallurgical and Materials Transactions A, 1990, 21(2): 557–565.
- [3] KATO M, NISHIO K, YAMAGUCHI T, NOKAMI T. Investigation of feathery crystals developed in weld metal in aluminum alloys by SAM and TEM [J]. Welding International, 1997, 11(8): 633–638.
- [4] CHEN Ti-jun, LI Xiang-wei, GUO Hai-yang, HAO Yuan. Microstructure and crystal growth direction of Al–Cu alloy [J]. Transactions of Nonferrous Metals Society of China, 2015, 25(5): 1399–1409.
- [5] TURCHIN A N, ZUIJDERWIJK M, POOL J, ESKIN D G, KATGERMAN L. Feathery grain growth during solidification under forced flow conditions [J]. Acta Materialia, 2007, 55(11): 3795–3801.
- [6] MATSUSHI F, HONMA U, OYA S. Theory of origin and multiplication of growth twin crystals in aluminum and aluminum-base alloys: Studies on growth twin crystals in aluminum and aluminum-base alloys (2nd Report) [J]. Journal of Japan Institute of Light Metals, 1969, 19(7): 287–298.
- [7] KURTULDU G, JARRY P, RAPPAZ M. Influence of Cr on the nucleation of primary Al and formation of twinned dendrites in Al–Zn–Cr alloys: Can icosahedral solid clusters play a role? [J]. Acta Materialia, 2013, 61(19): 7098–7108.
- [8] NAKATANI Y, SHIMIZU K, FUKUDA K, HASHIMOTO T. Effects of alloying components and conditions of solidification on the formation of feathery crystals in aluminum alloys: On feathery crystals in aluminum alloys (2nd Report) [J]. Journal of Japan Institute of Light Metals, 1968, 18(7): 1287–1296.
- [9] HOSOYA Y, URABE S. A study on the mechanism of nucleation and growth of twin tabular AgBr crystals [J]. Journal of Imaging Science and Technology, 1998, 42(6): 487–494.
- [10] SALGADO-ORDORICA M A, RAPPAZ M. Twinned dendrite growth in binary aluminum alloys [J]. Acta Materialia, 2008, 56(19): 5708–5718.
- [11] GULLMAN L O, JOHANSSON L. Factors governing the formation of feathery crystals in DC-cast ingots [M]. Hoboken, NJ, USA: John Wiley & Sons, Inc, 2013: 438–451.
- [12] HENRY S, GRUEN G U, RAPPAZ M. Influence of convection on feathery grain formation in aluminum alloys [J]. Metallurgical and Materials Transactions A, 2004, 35(8): 2495–2501.
- [13] HENRY S, MINGHETTI T, RAPPAZ M. Dendrite growth morphologies in aluminum alloys [J]. Acta Materialia, 1998, 46(18): 6431–6443.
- [14] HENRY S, RAPPAZ M, JARRY P.  $\langle 110 \rangle$  dendrite growth in aluminum feathery grains [J]. Metallurgical and Materials Transactions A, 1998, 29(11): 2807–2817.
- [15] EADY J A, HOGAN L M. Some crystallographic observations of growth-twinned dendrites in aluminum [J]. Journal of Crystal Growth, 1974, 23(2): 129–136.
- [16] KATO H, CAHOON J R. Heterogeneous nucleation model of twinned crystal growth from the melt [J]. Metallurgical and Materials Transactions A, 1985, 16(4): 690–692.
- [17] SALGADO-ORDORICA M A, BURDET P, CANTONI M, RAPPAZ M. Study of the twinned dendrite tip shape II: Experimental assessment [J]. Acta Materialia, 2011, 59(13): 5085–5091.
- [18] YANG Rong-xian, LIU Zhi-yi, YING Pu-you, LI Jun-lin, LIN Liang-hua, ZENG Su-min. Multistage-aging process effect on formation of GP zones and mechanical properties in Al–Zn–Mg–Cu alloy [J]. Transactions of Nonferrous Metals Society of China, 2016, 26(5): 1183–1190.
- [19] GONZALES F, RAPPAZ M. Dendrite growth directions in aluminum-zinc alloys [J]. Metallurgical and Materials Transactions A, 2006, 37(9): 2797–2806.
- [20] SALGADO M A. Study of twinned dendrite growth stability [J]. Scripta Materialia, 2009, 61(4): 367–370.
- [21] SALGADO-ORDORICA M A, PHILLION A B, RAPPAZ M. Morphology and growth kinetic advantage of quenched twinned dendrites in Al–Zn Alloys [J]. Metallurgical and Materials Transactions A, 2013, 44(6): 2699–2706.
- [22] ANADA H, HAGINAKA R, TADA S, HORI S. Formation of feathery crystals in Al–Si alloys [J]. Materials Transactions, 2007, 30(9): 684–694.
- [23] NAGASHIO K, KURIBAYASHI K. Growth mechanism of twin-related and twin-free facet Si dendrites [J]. Acta Materialia, 2005, 53(10): 3021–3029.
- [24] KURZ W, FISHER D J. Fundamentals of solidification [M]. Aedermansdorf, Switzerland: Trans Tech Publications, 1989: 71–92.
- [25] SAROCH M, DUBEY K S, RAMACHANDRARAO P. On the composition dependence of faceting behaviour of primary phases during solidification [J]. Journal of Crystal Growth, 1993, 126(4): 701–706.
- [26] GUDGEL K A, JACKSON K A. Oscillatory growth of directionally solidified ammonium chloride dendrites [J]. Journal of Crystal Growth, 2001, 225(2–4): 264–267.

# 定向凝固 Al–32%Zn 合金孪生枝晶的形成

陈忠伟, 高建平

西北工业大学 凝固技术国家重点实验室, 西安 710072

**摘要:** 使用光学金相显微镜和电子背散射衍射技术研究定向凝固 Al–32%Zn(质量分数)合金组织中与等轴晶共存的孪生枝晶的形成和晶体学取向关系。结果表明: 合金的宏观组织表现为典型的羽毛状和扇状结构, 而显微组织是由共格和非共格孪晶界分隔的细长层片晶组成。孪生枝晶的初生主干和侧臂沿着 $\langle 110 \rangle$ 方向生长, 这不同于 $\alpha(\text{Al})$ 常规的 $\langle 100 \rangle$ 生长取向。当局部对流较弱时, 孪生枝晶的起源与固/液界面处晶体小平面生长有关。较大的温度梯度和中等凝固速率明显有利于孪生枝晶的形成。用图示方式描述了新孪晶界形成的3种增殖机制和孪晶面中枝晶的一种演变方式。

**关键词:** 定向凝固; 孪生枝晶; 生长方向; 铝合金

(Edited by Wei-ping CHEN)